Table of Contents

List of Figures

Chapter 1

Asymptotic analysis of radiative extinction: effect of soot addition on extinction limits of luminous laminar counterflow diffusion flames

1.1 Introduction

The objective of the present chapter is to use large activation energy asymptotic (AEA) theory to bring basic information on the extinction limits of non-premixed flames under sooting and radiating conditions, identical to the numerical configuration presented in previous chapters. The AEA analysis assumes single-step global combustion chemistry, constant heat capacity and unity Lewis numbers; it also includes a two-equation phenomenological model to describe soot formation, growth and oxidation processes, as well as a generalized treatment of thermal radiation that assumes spectrally-averaged gray-medium properties and applies to flames with an arbitrary optical thickness. The focus of the present study is on the effect of external soot loading on flame extinction, and in particular on the slow-mixing/radiative-extinction limit that is believed to be the dominant mechanism that determines flame extinction in fires. External soot loading simulates non-local effects observed in multi-dimensional sooting flames in which soot mass may be produced at some flame locations and transported to others where it will increase the flame luminosity and drive combustion conditions towards extinction.

The AEA analysis shows that external soot loading results in a significant decrease of the size of the flammable domain and that the minimum value of flame stretch at the radiative extinction limit is increased by more than one order of magnitude compared to a non-soot-loaded-flame case. Multi-dimensional sooting flames are therefore expected to be significantly more susceptible to radiative extinction than the one-dimensional configurations that have been previously studied in microgravity combustion research.

Laminar diffusion flames may be extinguished by a number of different mechanisms. For instance, diffusion flames may be extinguished by aerodynamic quenching, a mechanism in which the flame is weakened by fast flow-induced perturbations and a critical decrease in the flame residence time. Diffusion flames may also be extinguished by thermal quenching, a mechanism in which the flame is weakened by heat losses (e.g., convective cooling to cold wall surfaces, radiative cooling, or water evaporative cooling in fire suppression applications, etc) or by dilution quenching, a mechanism in which the flame is weakened due to changes in the fuel or oxidizer stream composition (e.g., air vitiation in under-ventilated fires); in both thermal and dilution quenching, extinction occurs because of a critical increase in the flame chemical time. Laminar flame theory suggests that all these different phenomena may be explained by a single flame extinction criterion known as a Damköhler number criterion [13, 27, 22]: the Damköhler number Da is defined as the ratio of a characteristic fuel-air mixing time divided by a characteristic chemical time and extinction is predicted to occur for values of Da that are critically low. The existence of several flame extinction mechanisms explains the different extinction limits that

are often observed in non-premixed combustion systems. For instance, in the classical gaseous-fuel laminar counterflow diffusion flame configuration, the domain of flammability is limited by two fundamental limits: a fast mixing limit and a slow mixing limit [9, 8, 17, 2, 14, 25, 19]. In the fast mixing limit, Da is small because the mixing time is short. The fast-mixing/aerodynamic-quenching limit is the classical limit observed in the high Reynolds number turbulent flames that are typical of many combustion engine applications. In contrast, in the slow mixing limit, Da is small because the heat release rate is moderate and thermal radiation effects are significant, the flame temperature is consequently low and the chemical time is long. The slow-mixing/radiative-extinction limit is believed to be the dominant mechanism for extinction in the low-to-moderate Reynolds number turbulent flames that are typical of fire applications.Radiative extinction has been studied in great detail over the past two decades in several laminar diffusion flame configurations, including solid fuel stagnation-point flames [23], spherical flames around liquid fuel droplets , and spherical or planar gaseous fuel flames [9, 8, 17, 2, 14, 25, 19] (see [13] for a review). Note that these previous studies correspond to microgravity conditions and to one-dimensional flame configurations; they are also characterized by extremely low values of the fuel-air mixing rates (i.e. low values of flame stretch). In microgravity configurations, radiative extinction is achieved by gradually decreasing the flame stretch and thereby promoting sluggish combustion conditions that are vulnerable to radiative cooling. The values of flame stretch at the radiative extinction limit are significantly lower than those found in earth-gravity laminar flames in which buoyancy-driven mixing will maintain a minimum value of the fuel-air mixing inten-

sity; therefore, the implications of the results obtained in microgravity configurations to earth-gravity-flames in general, and to turbulent combustion applications in particular remain entirely open questions. Note also, that in one-dimensional flame configurations, due to the very low flame temperatures observed at the radiative extinction limit (as low as 1100-1300 K), laminar flames become blue-colored and soot-free prior to extinction and that extinction is controlled by radiant emissions from gaseous species (primarily CO_2 and H_2O. The implications of these results to fire applications that emphasize the dominant role of soot and luminous radiation remain also unclear. The generic configuration used in the fire science literature to understand flame extinction is a laminar co-flow jet diffusion flame configuration at smoke point conditions [15, 16, 20]. In a laminar jet diffusion flame configuration (and assuming a sooty fuel), flame extinction is observed by gradually increasing the fuel flow rate and thereby lengthening the flame and promoting formation and growth of soot particles upstream of the flame surface. The smoke point corresponds to the transition from sooting flame conditions in which soot particles are completely oxidized in the vicinity of the flame surface to smoking flame conditions in which a fraction of the soot mass leaks across the reaction zone and is emitted downstream of the flame without oxidation. This transition is generally interpreted as a radiative extinction event [11] but note that unlike the extinction results obtained in microgravity configurations, soot is the dominant factor that controls the smoke point. One important feature of smoke point configurations is that the flame is two-dimensional; multi-dimensional effects are likely to play a major role in the flame dynamics: for instance, the soot produced at low-elevation high-temperature

flame locations is transported into the higher-elevation lower-temperature flame tip region where it contributes to weaken the combustion. This non-local soot loading effect is not present in classical one-dimensional configurations, which suggests that these configurations are not representative of multi-dimensional (laminar or turbulent) sooting flame conditions.The objective of the present study is to evaluate the effect of non-local soot loading on the extinction limits of diffusion flames. The configuration corresponds to steady, one-dimensional, planar, laminar, counterflow, diffusion flames; the fuel is ethylene and the oxidizer is air; soot loading is simulated by adding a controlled amount of soot mass to the flow upstream of the flame. We use an extended large Activation Energy Asymptotic (AEA) analysis to calculate the extinction limits; the AEA analysis is extended to include finite rate soot chemistry and a generalized treatment of thermal radiation that applies to participating media ranging from optically-thin to optically-thick. The AEA formulation and modeling choices are described in 2; results are then presented in 3.

1.2 Problem formulation

The problem uses conventional treatment using singular perturbation, the so called Activation Energy Asymptotics (AEA) approach, in which the flame is decomposed into the outer and inner regions and resolved by matched asymptotic expansions. The problem of interest is a counterflow diffusion flame, with fuel (Ethylene) and oxidizer (air) being supplied from the left and right respectively. This non-premixed combustion system is assumed to be described by a single-step

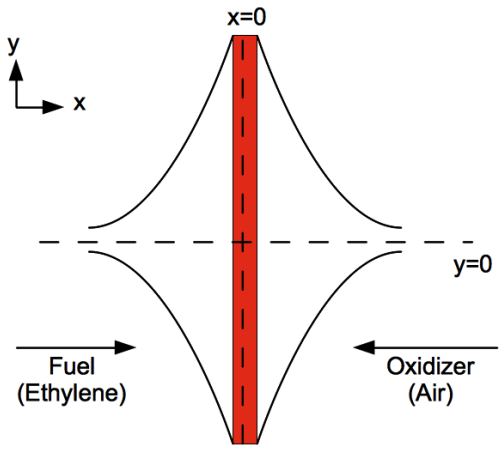

Figure 1.1: Schematic of counterflow flame. The flame is located to the right of the stagnation plane

global chemical reaction [26] as follows .

$$C_2H_4 + 3O_2 \rightarrow 2CO_2 + 2H_2O$$

1.3 Governing equations

The equations comprise those of mass, momentum and energy, as would be expected for a gas phase combustion problem. Transformations are made appropriately to simplify the treatment for variable density for the outer non-reacting scales using the Howarth transformation; and a flamelet type transformation at the inner regions in mixture fraction space. In addition to these, the radiation transfer equation is also solved in order to resolve radiation absorption.

1.3.1 Howarth transformation

Density weighted coordinates are used, in conformity with Carrier, Fendell and Marble [7] that greatly simplifies the analysis. The transformation is described here in brief. For more extensive notes, Dr. Howard Baum's [3] document may be referred to.

Consider a two dimensional counterflow flame configuration in which the flame normal is along the x direction; u and v being the velocities in the x and y directions and ρ being the density. The equation of continuity is

$$\frac{\partial \rho}{\partial t} + \frac{\partial (\rho u)}{\partial x} + \frac{\partial (\rho v)}{\partial y} = 0 \tag{1.1}$$

A mass weighted coordinate ξ is defined as

$$\xi = \int_0^x \frac{\rho}{\rho_2} \mathrm{d}x \tag{1.2}$$

where ρ_2 is the density of the oxidizer stream, which is denoted by the subscript 2, while $x = 0$ is the location of the stagnation plane. Transform the equations into this coordinate system comprised of $X = \xi$,$Y = y$ and $\mathcal{T} = t$ with the following transformation rules

$$\begin{aligned} x = x(\xi, Y, \mathcal{T}) \Rightarrow \frac{\partial}{\partial x} &= \frac{\partial}{\partial \xi}\frac{\partial \xi}{\partial x} + \frac{\partial}{\partial Y}\frac{\partial Y}{\partial x} + \frac{\partial}{\partial \mathcal{T}}\frac{\partial \mathcal{T}}{\partial x} \\ &= \frac{\partial}{\partial \xi}\frac{\partial \xi}{\partial x} \\ &= \frac{\rho}{\rho_2}\frac{\partial}{\partial \xi} \end{aligned} \tag{1.3}$$

$$\begin{aligned} y = y(\xi, Y, t) \Rightarrow \frac{\partial}{\partial y} &= \frac{\partial}{\partial \xi}\frac{\partial \xi}{\partial y} + \frac{\partial}{\partial Y}\frac{\partial Y}{\partial y} + \frac{\partial}{\partial \mathcal{T}}\frac{\partial \mathcal{T}}{\partial y} \\ &= \frac{\partial}{\partial \xi}\frac{\partial \xi}{\partial y} + \frac{\partial}{\partial Y} \end{aligned} \tag{1.4}$$

$$t = t(\xi, Y, \mathcal{T}) \Rightarrow \frac{\partial}{\partial t} = \frac{\partial}{\partial \xi}\frac{\partial \xi}{\partial t} + \frac{\partial}{\partial Y}\frac{\partial Y}{\partial t} + \frac{\partial}{\partial \mathcal{T}}\frac{\partial \mathcal{T}}{\partial t} = \frac{\partial}{\partial \xi}\frac{\partial \xi}{\partial t} + \frac{\partial}{\partial \mathcal{T}} \tag{1.5}$$

The continuity equation becomes, together with equation (1.2)

$$\frac{\partial}{\partial x}(\rho u + \rho_2 \frac{\partial \xi}{\partial t}) + \frac{\partial(\rho v)}{\partial y} = 0 \tag{1.6}$$

Now one may define a stream function $\psi(x, y, t)$ as follows

$$\rho_2 \frac{\partial \psi}{\partial x} = \rho v; \qquad \rho_2 \frac{\partial \psi}{\partial x} = -(\rho u + \rho_2 \frac{\partial \xi}{\partial t}) \tag{1.7}$$

Together with equation (1.2) the this gives

$$\frac{\partial \psi}{\partial \xi} = v \tag{1.8}$$

One can now define a normal transformed velocity $U(\xi, Y, \mathcal{T})$ as

$$\frac{\partial \psi}{\partial Y} = -U \tag{1.9}$$

A constant density version of the continuity equation may now be written as

$$\frac{\partial v}{\partial Y} + \frac{\partial U}{\partial \xi} = 0 \tag{1.10}$$

The velocity U is obtained from the equation (1.7) as

$$U = \frac{1}{\rho_2}\frac{\partial \xi}{\partial t} + \frac{\rho}{\rho_2}u + v\frac{\partial \xi}{\partial y} \tag{1.11}$$

The continuity equation may now be cast into a form, after suitable manipulation, to preserve the convective derivative to obtain

$$\frac{\mathrm{D}}{\mathrm{D}t} = \frac{\partial}{\partial \mathcal{T}} + U\frac{\partial}{\partial \xi} + v\frac{\partial}{\partial Y} \equiv \frac{\tilde{\mathrm{D}}}{\tilde{\mathrm{D}}\mathcal{T}} \tag{1.12}$$

1.3.2 Applying Howarth transform to governing equations

The governing equations are manipulated by invoking one-dimensionality, so that all quantities (except the velocities) vary only in the x direction, which is normal to the flame. The velocity in the direction normal to the flame in this new coordinate system is obtained from the equation (1.10) as

$$U = -\int_0^{\xi} \frac{\partial v}{\partial Y} \mathrm{d}\xi \tag{1.13}$$

If a constant strain rate $\partial v/\partial Y = \alpha$, together with a reference velocity of zero at $\xi = 0$ is assumed, one gets at the stagnation plane location $x = 0$

$$U = \int_0^{\xi} \frac{\partial v}{\partial Y} \mathrm{d}\xi = -\alpha\xi \tag{1.14}$$

In the undermentioned, $\mathcal{T}$ and Y are replaced later by t and y to retain the usual notation. The transport operator is now transformed into mass weighted coordinates. As mentioned in the foregoing, quantities of interest are only assumed to depend on x and t. Furthermore, unity Lewis numbers are assumed so that the diffusion coefficient may be denoted by a quantity D. Define a tranpsort ooperator L as follows

$$\rho L \equiv \rho\frac{\partial}{\partial t} + \rho u\frac{\partial}{\partial x} - \frac{\partial}{\partial x}\left(D\rho\frac{\partial}{\partial x}\right) - \frac{\partial}{\partial y}\left(D\rho\frac{\partial}{\partial y}\right) \tag{1.15}$$

Upon introducing the Howarth transformation (1.2), and ignoring Y dependence, one gets

$$\rho\frac{\partial}{\partial t} + \rho u\frac{\partial}{\partial x} = \rho\left(\frac{\partial}{\partial \mathcal{T}} - \alpha\xi\frac{\partial}{\partial \xi}\right) \tag{1.16}$$

The diffusion terms are manipulated, using the transformation (1.2) as follows

$$\begin{aligned}\frac{\partial}{\partial x}\left(\rho D\frac{\partial}{\partial x}\right) &= \frac{\rho}{\rho_2}\frac{\partial}{\partial \xi}\left(D\rho\frac{\rho}{\rho_2}\frac{\partial}{\partial \xi}\right)\\ &= \frac{\rho}{\rho_2^2}\frac{\partial}{\partial \xi}\left(D\rho^2\frac{\partial}{\partial \xi}\right)\end{aligned} \tag{1.17}$$

Now, if one makes the simplification that $D\rho^2$ is nearly constant in flows of interest, one may remove this quantity as $D\rho^2 = D_2\rho_2^2$. One may replace $\mathcal{T}$ with t to obtain

$$L \equiv \frac{\partial}{\partial t} - \alpha\xi\frac{\partial}{\partial \xi} - D_2\frac{\partial^2}{\partial \xi^2} \tag{1.18}$$

1.3.3 Non-dimensionalization

The governing equations for species mass and energy are

$$\begin{aligned}\rho L(Y_F) &= -\dot{\omega}_F\\ \rho L(Y_{O_2}) &= -r_s\dot{\omega}_F\\ \rho L(h) &= \Delta H_F\dot{\omega}_F + \nabla\cdot\vec{q}_R\end{aligned} \tag{1.19}$$

where Y_F, Y_{O_2} are the fuel and oxidizer mass fractions respectively; $h = \int_0^T c_p \mathrm{d}T = c_pT$ the enthalpy for material at temperature T, for a constant specific heat $c_p = 1008$ J/kg − k, based on some reference enthalpy at temperature $T_0 = 0$; $\Delta H_F = 32.7$ MJ/kg is the heat of combustion per unit mass of fuel (a positive quantity); $\dot{\omega}_F$ is the fuel mass burning rate per unit volume; r_s is the stoichiometric fuel-air coefficient in the chemical reaction. The non-dimensional quantities are

superscripted by primes

$$\rho' = \frac{\rho}{\rho_2}; \qquad \xi' = \frac{\xi}{\ell}; \qquad t' = \alpha t$$
$$Y_F' = \frac{Y_F}{Y_{F,1}}; \qquad Y_{O_2}' = \frac{Y_{O_2}}{r_s Y_{F,1}}; \qquad Y_{CO_2}' = \frac{Y_{CO_2}}{r_{CO_2} Y_{F,1}} \tag{1.20}$$
$$Y_{H_2O}' = \frac{Y_{H_2O}}{r_{H_2O} Y_{F,1}}; \qquad T' = \frac{c_p T}{\Delta H_F Y_{F,1}}$$

In the foregoing equations, ℓ is a reference convective length scale (to be defined), and quantities subscripted with $1, 2$ are reference quanties at the fuel and oxidizer boundaries respectively: $Y_{F,1} = Y_F(\xi = -\infty)$, $\rho_2 = \rho(\xi = \infty)$. The convective length scale ℓ is defined based on the aforementioned quantities as

$$\ell = \sqrt{\frac{D_2}{\alpha}} \tag{1.21}$$

In the foregoing, the oxidizer stream's diffusivity is $D_2 = 2.21 \times 10^{-5}$ m^2/s. The reaction term is taken to be of the following form, proposed in [26]

$$\dot{\omega}_F = \frac{A}{(10^6)^{p+q-1}} \times M_F \left(\frac{\rho Y_F}{M_F}\right)^p \left(\frac{\rho Y_{O_2}}{M_{O_2}}\right)^q \exp\left(-\frac{T_a}{T}\right) \tag{1.22}$$

where $A = 2.0 \times 10^{12}$ (mol/m^3)$^{1-\mathrm{p}-\mathrm{q}}$ s^{-1} is a model coefficient, p, q are the model fuel and oxidizer exponents, $p = 0.1$, $q = 1.65$, M_k the molecular weight of species k (kg/mol), and T_a a model activation temperature, $T_a = 15107$ K. Collecting terms in the above equation so that

$$B = \frac{A}{(10^6)^{p+q-1}} M_F \tag{1.23}$$

the reaction source term $\dot{\omega}_F$ may be written as

$$\dot{\omega}_F = B \left(\frac{\rho Y_F}{M_F}\right)^p \left(\frac{\rho Y_{O_2}}{M_{O_2}}\right)^q \exp\left(-\frac{T_a}{T}\right) \tag{1.24}$$

1.4 Solution approach

The governing equations are solved using matched asymptotic expansions [4] in conventional fashion. Here, the outer regions comprise the radiatively active layer, while the inner region is the thin reacting zone, which forms a *corner* boundary layer whose location is to be determined (which, however, may be intuitively viewed as the region where fuel and oxidizer mix at stoichiometric proportions). It is apparent from the above, that the length scale for radiation is much larger than that of the reaction zone. Also, it is therefore borne out that the radiation term is dwarfed by the reaction term inside the inner layer (except, perhaps in regions where the optical thickness is large, which is not considered presently). The outer and inner problems are thus posed by appropriately expressing the governing equations. They are then matched to arrive at the complete solution.

1.5 Outer solutions

The outer solutions are derived as follows, using the Howarth transformed equation (1.18).

$$\begin{aligned} \rho L(Y_F) &= -\dot{\omega}_F \\ \rho L(Y_{O_2}) &= -r_s \dot{\omega}_F \\ \rho L(h) &= \Delta H_F \dot{\omega}_F + \nabla \cdot \vec{q}_R \end{aligned} \tag{1.25}$$

where

$$L \equiv -\alpha\xi \frac{\mathrm{d}}{\mathrm{d}\xi} - D_2 \frac{\mathrm{d}^2}{\mathrm{d}\xi^2} \tag{1.26}$$

In the above, the time dependency is removed since the problem under consideration is a steady counterflow flame. However, it may be added if desired.

After non-dimensionalizing, and abstracting the reaction source term into a Dirac-delta function $\delta(\xi - \xi_f)$, which is zero everywhere, except at the flame located at ξ_f where it is infinite, one gets

$$\begin{aligned} \rho L'(Y'_F) &= A_r \delta(\xi - \xi_f) \\ \rho L'(Y'_{O_2}) &= A_r \delta(\xi - \xi_f) \\ \rho L'(T') &= -A_r \delta(\xi - \xi_f) + \frac{1}{\Delta H_F \alpha Y_{F,1}} \nabla \cdot \vec{q}_R \end{aligned} \tag{1.27}$$

where

$$L' \equiv -\xi' \frac{\mathrm{d}}{\mathrm{d}\xi'} - \frac{\mathrm{d}^2}{\mathrm{d}\xi'^2} \tag{1.28}$$

and A_r is a quantity that denotes the strength of the chemical reaction (added for consistency reasons).

In the forthcoming developments, a non-dimensional notation for the outer variables of interest is defined as follows

$$\begin{gathered} \xi' \to \zeta; \qquad L' \to \hat{L}; \qquad Y'_F \to \hat{Y}_F \\ Y'_{O_2} \to \hat{Y}_{O_2}; \qquad Y'_{CO_2} \to \hat{Y}_{CO_2}; \qquad Y'_{H_2O} \to \hat{Y}_{H_2O}; \\ T' \to \hat{T}; \qquad \rho' \to \hat{\rho} \end{gathered} \tag{1.29}$$

With these definitions, the outer equations are rewritten as

$$\begin{aligned} \hat{L}(\hat{Y}_F) &= 0 \\ \hat{L}(\hat{Y}_{O_2}) &= 0 \\ \hat{L}(\hat{T}) &= \frac{1}{\alpha \hat{\rho}} \nabla \cdot \vec{q}_R \end{aligned} \tag{1.30}$$

subject to the boundary conditions

$$\begin{gathered}\hat{Y}_F(-\infty) = Y'_F(-\infty) = Y'_{F,-\infty}; \qquad \hat{Y}_F(\infty) = Y'_F(\infty) = Y'_{F,\infty} = 0 \\ \hat{Y}_{O_2}(-\infty) = Y'_{O_2}(-\infty) = Y'_{O_2,-\infty} = 0; \qquad \hat{Y}_{O_2}(\infty) = Y'_{O_2}(\infty) = Y'_{O_2,\infty} \\ \hat{T}(-\infty) = T'(-\infty) = T'_{-\infty}; \qquad \hat{T}(\infty) = T'(\infty) = T'_{\infty}\end{gathered} \tag{1.31}$$

It is noted that the reaction source term, contained in the Dirac-delta function is non-existent in the outer equations. However, since these equations are solved on either side of the flame, one needs to know the values taken by the variables at the flame, which is done in the forthcoming.

1.5.1 Flame location

The flame location is determined using the Shvab-Zeldovich coupling relationships contained in equations (1.27).

$$L'(Y'_F - Y'_{O_2}) = 0 \tag{1.32}$$

The quantity in the paranthesis $Y'_F - Y'_{O_2}$ is well behaved thoughout the domain and varies in the outer scale. Using appropriate boundary conditions for fuel and oxidizer (which are entirely known), one may solve the above equation to get

$$Y'_F - Y'_{O_2} = \frac{Y'_{F,-\infty} - Y'_{O_2,\infty}}{2} - \frac{Y'_{F,-\infty} + Y'_{O_2,\infty}}{2} \operatorname{erf}\left(\frac{\xi'}{\sqrt{2}}\right) \tag{1.33}$$

The flame location is taken to be that where fuel and oxidizer both simultaneously vanish to leading order. If this is used in the foregoing equation, one gets

$$\operatorname{erf}\left(\frac{\xi'_f}{\sqrt{2}}\right) = \frac{Y'_{F,-\infty} - Y'_{O_2,\infty}}{Y'_{F,-\infty} + Y'_{O_2,\infty}} \tag{1.34}$$

which gives the flame location. It is noted that this occurs at the stoichiometric location, as it would even without radiation heat losses. The flame location is henceforth denoted by the subscript st. Also, the quantity on the LHS of equation (1.33) is essentially a restatement of the mixture fraction, defined below so that the mixture fraction Z is zero at the air stream, and unity at the fuel stream.

$$Z = \frac{Y'_F - Y'_{O_2} + Y'_{O_2,\infty}}{Y'_{F,-\infty} + Y'_{O_2,\infty}} \tag{1.35}$$

The mixture fraction profile may then be expressed by the relationship

$$Z = \frac{1}{2}\left[1 - \text{erf}\left(\frac{\xi'}{\sqrt{2}}\right)\right] \tag{1.36}$$

1.5.2 Quantities at the flame location

This is done analogously to the above.

$$L'(Y'_F + T'^0) = 0 \tag{1.37}$$

where T'^0 is the non-dimensional flame temperature (the outer solutions of which are which are expressed in the same notation as defined in the foregoing) in the absence of radiation. This is the so called Burke-Schuman flame temperature for the adiabatic flame. One gets the adiabatic flame temperature upon solving this equation and substituting for values at the stoichiometric location.

The boundary conditions for the foregoing equation are

$$\begin{aligned} Y'_{F,-\infty} = Y'_F(-\infty); \qquad Y'_{F,\infty} = Y'_F(\infty) \\ T^{0\prime}(-\infty) = T'(-\infty); \qquad T^{0\prime}(\infty) = T'(\infty) \end{aligned} \tag{1.38}$$

The solution can be written as

$$T^{0\prime} + Y'_F = \frac{T'_\infty - T'_{-\infty} - Y'_{F,-\infty}}{2} \operatorname{erf}\left(\frac{\xi'}{\sqrt{2}}\right) + \frac{T'_{-\infty} + T'_\infty + Y'_{F,-\infty}}{2} \tag{1.39}$$

The flame location can be inserted from equation (1.34), after recognizing that $\hat{Y}_{F,st} = 0$, to get the non-dimensional adiabatic flame temperature $\hat{T}^0_{st}$ as

$$\hat{T}^0_{st} = \frac{T'_\infty - T'_{-\infty} - Y'_{F,-\infty}}{2} \left(\frac{Y'_{F,-\infty} - Y'_{O_2,\infty}}{Y'_{F,-\infty} + Y'_{O_2,\infty}}\right) + \frac{T'_{-\infty} + T'_\infty + Y'_{F,-\infty}}{2} \tag{1.40}$$

In similar fashion, one may also obtain the values at the flame location for other quantities, such as $\hat{Y}_{CO_2,st}$ and $\hat{Y}_{H_2O,st}$.

1.5.3 Non-radiating solutions

The solutions to the non-radiating problem are to be obtained for use in the radiating problem. These are the so called Burke-Schuman solutions for the unstrained problem far from the reaction zone.

The equations to be solved are

$$\begin{aligned} \hat{L}(\hat{Y}_F) &= 0 \\ \hat{L}(\hat{Y}_{O_2}) &= 0 \\ \hat{L}(\hat{Y}_{CO_2}) &= 0 \\ \hat{L}(\hat{Y}_{H_2O}) &= 0 \\ \hat{L}(\hat{T}^0) &= 0 \end{aligned} \tag{1.41}$$

$\hat{T}^0$ is the *outer* 'adiabatic' or radiation free solution to the outer energy equation. This must be distinguished from $\hat{T}$, which also contains within it the effects of

radiation. The species mass fractions remain the same in both the radiating and non-radiating solutions because their outer equations are unchanged in the presence of radiation. However, the energy equation will have to be revisited because alterations are effected by the radiation source term.

The outer solutions are characterized by a slope discontinuity on either side of the flame, which will have to be corrected by patching with the inner solution. The non-radiating solutions may be written as follows

$$\begin{aligned} \hat{Y}_F &= Y'_{F,-\infty} \frac{\text{erf}\left(\frac{\zeta_{st}}{\sqrt{2}}\right) - \text{erf}\left(\frac{\zeta}{\sqrt{2}}\right)}{1 + \text{erf}\left(\frac{\zeta_{st}}{\sqrt{2}}\right)}; && \zeta < \zeta_{st} \\ &= 0; && \zeta \geq \zeta_{st} \end{aligned} \tag{1.42}$$

$$\begin{aligned} \hat{Y}_{O_2} &= 0; && \zeta < \zeta_{st} \\ &= Y'_{O_2,\infty} \frac{\text{erf}\left(\frac{\zeta}{\sqrt{2}}\right) - \text{erf}\left(\frac{\zeta_{st}}{\sqrt{2}}\right)}{1 - \text{erf}\left(\frac{\zeta_{st}}{\sqrt{2}}\right)}; && \zeta \geq \zeta_{st} \end{aligned} \tag{1.43}$$

$$\begin{aligned} \hat{Y}_{CO_2} &= \hat{Y}_{CO_2,st} \frac{1 + \text{erf}\left(\frac{\zeta}{\sqrt{2}}\right)}{1 + \text{erf}\left(\frac{\zeta_{st}}{\sqrt{2}}\right)}; && \zeta < \zeta_{st} \\ &= \hat{Y}_{CO_2,st} \frac{\text{erf}\left(\frac{\zeta}{\sqrt{2}}\right) - \text{erf}\left(\frac{\zeta_{st}}{\sqrt{2}}\right)}{1 - \text{erf}\left(\frac{\zeta_{st}}{\sqrt{2}}\right)}; && \zeta \geq \zeta_{st} \end{aligned} \tag{1.44}$$

$$\begin{aligned} \hat{Y}_{H_2O} &= \hat{Y}_{H_2O,st} \frac{1 + \text{erf}\left(\frac{\zeta}{\sqrt{2}}\right)}{1 + \text{erf}\left(\frac{\zeta_{st}}{\sqrt{2}}\right)}; && \zeta < \zeta_{st} \\ &= \hat{Y}_{H_2O,st} \frac{\text{erf}\left(\frac{\zeta}{\sqrt{2}}\right) - \text{erf}\left(\frac{\zeta_{st}}{\sqrt{2}}\right)}{1 - \text{erf}\left(\frac{\zeta_{st}}{\sqrt{2}}\right)}; && \zeta \geq \zeta_{st} \end{aligned} \tag{1.45}$$

$$\begin{aligned}\hat{T}^0 &= \hat{T}^0_{st}\frac{1+\ \mathrm{erf}\left(\frac{\zeta}{\sqrt{2}}\right)}{1+\ \mathrm{erf}\left(\frac{\zeta_*}{\sqrt{2}}\right)} + T'_{-\infty}\frac{\mathrm{erf}\left(\frac{\zeta_{st}}{\sqrt{2}}\right)-\ \mathrm{erf}\left(\frac{\zeta}{\sqrt{2}}\right)}{1+\ \mathrm{erf}\left(\frac{\zeta_{st}}{\sqrt{2}}\right)}; \quad \zeta < \zeta_{st} \\ &= \hat{T}^0_{st}\frac{1-\ \mathrm{erf}\left(\frac{\zeta}{\sqrt{2}}\right)}{1-\ \mathrm{erf}\left(\frac{\zeta_{st}}{\sqrt{2}}\right)} + T'_{\infty}\frac{\mathrm{erf}\left(\frac{\zeta}{\sqrt{2}}\right)-\ \mathrm{erf}\left(\frac{\zeta_{st}}{\sqrt{2}}\right)}{1-\ \mathrm{erf}\left(\frac{\zeta_{st}}{\sqrt{2}}\right)}; \quad \zeta \geq \zeta_{st}\end{aligned} \tag{1.46}$$

1.5.4 Radiation source term

The radiation source term is given by the expression

$$\nabla \cdot \vec{q}_R = -\kappa(4\sigma T^4 - G) \tag{1.47}$$

where κ is the Planck mean absorption coefficient (described below) and G is the integrated incident radiation. κ comprises contributions from gas radiation (in this case, CO_2 and H_2O), and a contribution from soot luminosity (which is typically the dominant part).

$$\kappa = p(x_{\mathrm{CO_2}}a_{\mathrm{CO_2}} + x_{\mathrm{H_2O}}a_{\mathrm{H_2O}} + C_{soot}f_v T \tag{1.48}$$

where p is pressure (atm), x_k the mole fraction of species k, a_k is described by curve-fit expression given in [1]. C_{soot} is a quantity that may be tuned in order to make the medium more, or less radiating during numerical experiments, f_v is the soot volume fraction. Unless otherwise mentioned, a value of $C_{soot} = 1817\ \mathrm{m^{-1}K^{-1}}$ (based on recent measurements [**?**]) is used in the current work.

The two terms on the right hand side of Equation 1.47 are the contributions from emission and absorption. The emission term contains the T^4 dependence on flame temperature and is computable once we know that quantity. However, the radiation absorption term G is in general, non-local, although under special conditions

(optically thin flames) it may be approximated. But in a general case, one obtains it by solving the radiative transport equation (RTE), detailed in the following.

1.5.4.1 Obtaining radiation heat fluxes by solving RTE

An expression for radiant energy absorption is developed below for the laminar counterflow flame configuration. This expression may be used in the outer energy equation in order to compute the temperature field predicated by radiation losses.

The radiation transport equation in the absence of scattering is

$$\frac{\mathrm{d}I(s)}{\mathrm{d}s} = \kappa(s)(I_b(s) - I(s)) \tag{1.49}$$

where I is the intensity of a ray traveling in the direction $\hat{s}$, s being a coordinate defined in the direction of the ray's path, κ is the Planck mean absorption coefficient, $I_b = \sigma T^4/\pi$ being the black-body intensity at temperature T, with σ being the Stephen-Boltzmann constant. Since this is an entirely symmetric problem, one may alternatively recast the above in terms of x and the polar angle θ. The azimuthal angle ϕ will not appear in the expression because of symmetry, and will be integrated out. Note that the analysis now uses dimensional coordinates.

Considering an angle $0 < \theta < \pi/2$, one may write

$$\mathrm{d}x = -\frac{\mathrm{d}s}{\cos\theta} \tag{1.50}$$

and

$$-\cos\theta\frac{\mathrm{d}I}{\mathrm{d}x} = \kappa(I_b - I) \tag{1.51}$$

Define the optical thickness $\tau(x)$ as

$$\tau(x) = \int_0^x \kappa(x')\mathrm{d}x' \tag{1.52}$$

so that

$$\mathrm{d}\tau(x') = \kappa(x')\mathrm{d}x' \tag{1.53}$$

Also, define a shorthand notation for τ as follows

$$\tau = \tau(x), \qquad \tau' = \tau(x') \tag{1.54}$$

Multiplying both sides of equation (1.51) by $\exp(-\tau/\cos\theta)$ and grouping terms, one gets

$$\frac{\mathrm{d}}{\mathrm{d}\tau}\left[I\exp\left(-\frac{\tau}{\cos\theta}\right)\right] = \left(-\frac{I_b}{\cos\theta}\right)\exp\left(-\frac{\tau}{\cos\theta}\right) \tag{1.55}$$

which can be integrated as

$$\int_\infty^\tau \frac{\mathrm{d}}{\mathrm{d}\tau'}\left(Ie^{-\frac{\tau'}{\cos\theta}}\right)\mathrm{d}\tau' = -\int_\infty^\tau \frac{I_b}{\cos\theta}e^{-\frac{\tau'}{\cos\theta}}\mathrm{d}\tau' \tag{1.56}$$

giving

$$I[\tau(x)] = \int_{\tau(x)}^\infty \frac{I_b(\tau')}{\cos\theta}\exp\left(-\frac{\tau(x') - \tau(x)}{\cos\theta}\right)\mathrm{d}\tau' \tag{1.57}$$

This is only the contribution from the *right* of the point x. One may likewise derive an expression for the contribution from the left of x. The subscript $+$ and $-$ shall henceforth be used to mark this distinction.

1.5.4.2 Absorption source term

The absorption source term is derived by taking the integral of the intensity in solid angle space as follows

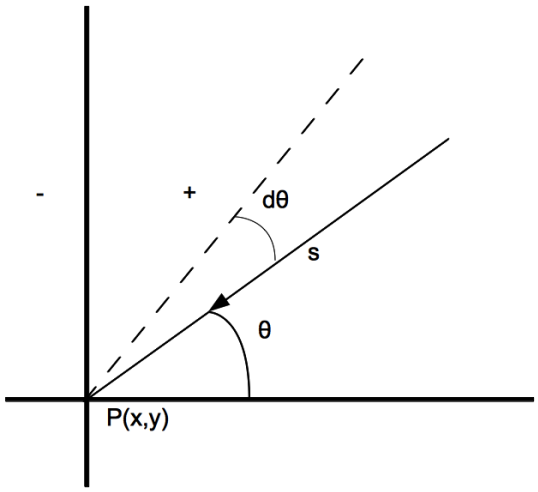

Figure 1.2: Schematic of domain and setup to calculate radiation absorption by integrating RTE. The left and right of the point under consideration $P(x, y)$ are denoted by '-' and '+' respectively.

$$S_{R,A} = \kappa G = \kappa \int_{\Omega} I \mathrm{d}\Omega \tag{1.58}$$

If one calls the contributions to the radiation source term from the left and right as q_- and q_+ respectively, one has

$$S_{R,A} = q_- + q_+ \tag{1.59}$$

The derivation for q_+ is shown in the following. q_- may be obtained similarly.

$$\begin{aligned} q_+ &= \int_0^{\frac{\pi}{2}} I_+(x) \sin\theta \mathrm{d}\theta \int_0^{2\pi} \mathrm{d}\phi \\ &= 2\pi\kappa \int_{\tau}^{\infty} \int_0^{\frac{\pi}{2}} \frac{I_b}{\cos\theta} \exp\left(-\frac{\tau' - \tau}{\cos\theta}\right) \sin\theta \mathrm{d}\tau' \mathrm{d}\theta \end{aligned} \tag{1.60}$$

One now makes the transformation

$$t = \frac{\tau' - \tau}{\cos\theta} \tag{1.61}$$

to get

$$q_+ = 2\pi\kappa \int_\tau^\infty I_b(\tau')\mathrm{E}_1(\tau' - \tau)\mathrm{d}\tau' \tag{1.62}$$

where E_1 is the exponential integral function defined as follows

$$\mathrm{E}_1(t) = \int_1^\infty \frac{\exp(-tz)}{z}\mathrm{d}z \tag{1.63}$$

One may similarly obtain the expression for q_- as

$$q_- = 2\pi\kappa \int_{-\infty}^\tau I_b(\tau')\mathrm{E}_1(\tau - \tau')\mathrm{d}\tau' \tag{1.64}$$

The radiation absorption source term $S_{R,A}$ then becomes

$$\begin{aligned} S_{R,A} &= q_+ + q_- \\ &= 2\pi\kappa \left(\int_{-\infty}^\tau I_b(\tau')\mathrm{E}_1(\tau - \tau')\mathrm{d}\tau' + \int_\tau^\infty I_b(\tau')\mathrm{E}_1(\tau' - \tau)\mathrm{d}\tau' \right) \end{aligned} \tag{1.65}$$

In an optically thin medium with a quasi constant temperature T_∞, and $\tau \to 0$ one may recover the well known expression

$$S_{R,A} = 4\pi\kappa I_b(T = T_\infty) \tag{1.66}$$

since $\int_0^\infty \mathrm{E}_1(x)\mathrm{d}x = 1$.

1.5.4.3 Transformation into the Howarth framework

Since the governing equations are expressed in terms of the density weighted coordinate ξ, one needs to transform the foregoing absorption heat source term into that framework. Recognizing that

$$\xi = \int_{-\infty}^x \frac{\rho(x')}{\rho_2}\mathrm{d}x' \tag{1.67}$$

and

$$\mathrm{d}\tau' = \kappa(x')\mathrm{d}x' \tag{1.68}$$

one can write the absorption heat source term (1.65) as

$$\begin{aligned} S_{R,A} = 2\pi\kappa(\xi) \int_{-\infty}^{\xi} I_b(\xi')\mathrm{E}_1[\tau(\xi) - \tau(\xi')]\kappa(\xi')\frac{\rho_2}{\rho(\xi')}\mathrm{d}\xi' \\ + 2\kappa(\xi)\pi \int_{\xi}^{\infty} I_b(\xi')\mathrm{E}_1[\tau(\xi') - \tau(\xi)]\kappa(\xi')\frac{\rho_2}{\rho(\xi')}\mathrm{d}\xi' \end{aligned} \tag{1.69}$$

1.5.5 Radiating solutions-solving for the outer temperature field

If the radiation source term is available, one may proceed with solving the outer equations to obtain the outer temperature field. It is clear that the mass fraction profiles are unaltered in the presence of radiation (since the outer equations are not any different from the case without radiation). The equations to be solved are as follows

$$\hat{L}(\hat{T}) = f(\zeta) \tag{1.70}$$

where f is the radiating term from equation 1.30)

$$f = \frac{\nabla \cdot \vec{q}_R}{\alpha\rho\Delta H_F Y_{F,1}} \tag{1.71}$$

The density is related to the temperature by means of the ideal gas law, at a constant atmospheric pressure P_∞.

$$P_\infty = \rho\frac{R}{M_{mix}}T \tag{1.72}$$

where R is the ideal gas constant, and M_{mix} is the molecular weight of the mixture at any given location.

$$M_{mix} = \frac{1}{\sum_k \frac{Y_k}{M_k}} \tag{1.73}$$

where M_k is the molecular weight of species k. The absorption coefficient κ_{outer} may be obtained by summing up contributions from each radiating species.

$$\hat{\kappa} = \hat{\kappa}_{\mathrm{CO_2}} + \hat{\kappa}_{\mathrm{H_2O}} + \hat{\kappa}_{soot} \tag{1.74}$$

where,

$$\kappa_{\mathrm{CO_2}} + \kappa_{\mathrm{H_2O}} = p(x_{\mathrm{CO_2}} a_{\mathrm{CO_2}} + x_{\mathrm{H_2O}} a_{\mathrm{H_2O}})$$

and

$$\kappa_{soot} = C_{soot} f_v T$$

Again, the outer temperatures are used to compute these quantities, except for soot which is sensitive to the inner structure, for which one uses the solutions obtained after solving for the quantities over the whole domain (details explained in 1.7).

1.5.6 Solving for outer temperature using Green's functions

For the sake of convenience, the outer temperature is expressed in terms of the temperature drop from adiabatic or non-radiating conditions.

$$\hat{T}(\zeta) = \hat{T}^0(\zeta) - \Delta\hat{T}(\zeta) \tag{1.75}$$

where $\Delta\hat{T}$ is the correction to the outer temperature due to radiation. This is a quantity that we assume to be continuous and *smooth* upto its second derivative. This would be the case if we have *complete* consumption of fuel and oxidizer (it becomes apparent on manipulating the governing equations, as is explained in the appendices). As shall be seen, the burning rate scales as the inverse square root of

the mixing rate, demonstrating that the assumption is correct. The outer energy equation now becomes

$$-\hat{L}(\Delta\hat{T}) = f(\zeta) \tag{1.76}$$

This is a non-linear equation in that the right-hand side depends on both the flame temperature. The treatment adopted is to linearize the right-hand side and solve the linearized equations with sequence of iterative sweeps. If $f(\zeta)$ *were* linear, we may solve this inhomogeneous equation using Green's functions as follows (the reader is referred to texts on ODEs for the pedagogical details [6]).

$$\Delta\hat{T}(\zeta) = \int_{-\infty}^{\infty} G(\zeta;t) f(t) \exp\left(\frac{t^2}{2}\right) \mathrm{d}t \tag{1.77}$$

where G is the Green's function for the ODE under consideration (Equation 1.76), which satisfies the boundary conditions of the original problem so that $\Delta\hat{T}^0(\zeta = \pm\infty) = 0$

$$\begin{aligned} G(\zeta,t) &= \frac{1}{2}\sqrt{\frac{\pi}{2}}\psi_1(t)\psi_2(\zeta); \qquad & t < \zeta \\ &= \frac{1}{2}\sqrt{\frac{\pi}{2}}\psi_2(t)\psi_1(\zeta); \qquad & t > \zeta \end{aligned} \tag{1.78}$$

where

$$\psi_1(\zeta) = \left[1 + \ \mathrm{erf}\left(\frac{\zeta}{\sqrt{2}}\right)\right] \tag{1.79}$$

and

$$\psi_2(\zeta) = \left[\ \mathrm{erf}\left(\frac{\zeta}{\sqrt{2}}\right) - 1\right] \tag{1.80}$$

1.5.7 Correction for nonlinearity using successive approximations

Having obtained the solutions to the linearized energy equation, one may proceed to correct for non-linearlity using successive approximations, so that the solu-

tion obtained during a given iteration may be used in the source term to get the next iterate of the solution, the procedure being repeated until there is no variation in the solution obtained. This is done as follows. Let $\hat{T}^N$ be the N^{th} iterate of the solution to the outer energy equation, written in terms of iterates as

$$-\hat{L}[\hat{T}^{N+1}(\zeta)] = f[\hat{T}^N(\zeta)] \tag{1.81}$$

where $\hat{T}$ is taken as the leading order solution for temperature, as implied in the foregoing sections. Given a known function $\hat{T}^N(\zeta)$, one can obtain $\hat{T}^{N+1}$ by using the Green's function approach indicated. One may continue this procedure until the difference between two successive iterates is smaller than a desired tolerance.

$$\frac{|\hat{T}^N - \hat{T}^{N+1}|}{|\hat{T}^N|} < tolerance \tag{1.82}$$

1.5.8 Relating 'Howarth' strain rate with the scalar dissipation rate

In the current work, the inner equations are solved in mixture fraction space. It is therefore of interest to relate the Howarth strain rate α with the scalar dissipation rate that appears in the inner equations. This is done as follows.

From the definition of the scalar dissipation rate at the flame in one dimensional coordinates χ_{st}, one has (with $x' = x/\ell$, the spatial coordinate, being non-dimensional)

$$\chi_{st} = \frac{2D_{st}}{\ell^2}\left(\frac{\mathrm{d}Z}{\mathrm{d}x'}\right)^2_{st} \tag{1.83}$$

Introducing the Howarth transformation implied in equation (1.2) one gets

$$\chi_{st} = \frac{2D_{st}}{\ell^2}\frac{\rho_{st}}{\rho_2}\left(\frac{\mathrm{d}Z}{\mathrm{d}\zeta}\right)^2_{st} \tag{1.84}$$

This may now be related to the Howarth strain rate α, recognizing that

$$\alpha = \frac{D_{st}}{\ell^2} \tag{1.85}$$

so that the scalar dissipation rate at the flame may be written as

$$\chi_{st} = 2\alpha \left(\frac{\rho_{st}}{\rho_2}\right)^2 \left(\frac{\mathrm{d}Z}{\mathrm{d}\zeta}\right)^2_{st} \tag{1.86}$$

The mixture fraction gradient is implied from the solution of the mixture fraction field Z, given by equation (1.36), reproduced below

$$Z = \frac{1}{2}\left[1 - \ \mathrm{erf}\left(\frac{\zeta}{\sqrt{2}}\right)\right] \tag{1.87}$$

Upon using this in the equation for the scalar dissipation rate (1.86), together with $\rho_{st}^2 D_{st} = \rho_2^2 D_2$ one gets the relationship between the strain rate and scalar dissipation rate as

$$\alpha = \pi \chi_{st} \exp(\zeta_{st}^2) \tag{1.88}$$

1.6 Inner equations

The inner equations at the reaction zone are solved in mixture fraction space. The notation for non-dimensional variables is such that one inserts a 'tilde' above each variable to represent its corresponding non-dimensional inner analogue.

$$T \to \tilde{T}; \qquad Y_F \to \tilde{Y}_F; \qquad Y_{O_2} \to \tilde{Y}_{O_2} \tag{1.89}$$

The governing equations for a one-dimensional, steady flamelet [21](under which assumptions the procedure is carried out) are as follows

$$\frac{\chi_{st}}{2}\frac{\mathrm{d}^2 Y_F}{\mathrm{d}Z^2} = \frac{\dot{\omega}_F}{\rho_{st}} \tag{1.90}$$

$$\frac{\chi_{st}}{2}\frac{\mathrm{d}^2 Y_{O_2}}{\mathrm{d}Z^2} = r_s\frac{\dot{\omega}_F}{\rho_{st}} \tag{1.91}$$

and

$$\frac{\chi_{st}}{2}\frac{\mathrm{d}^2 T}{\mathrm{d}Z^2} = -\frac{(\Delta H_F)}{c_p}\frac{\dot{\omega}_F}{\rho_{st}} + \frac{1}{\rho_{st}c_p}\nabla\cdot\vec{q}_R \tag{1.92}$$

The energy equation, after suitable non-dimensionalization, and neglecting the small radiation term (compared to reaction) may be written as

$$\frac{\mathrm{d}^2\tilde{T}}{\mathrm{d}Z^2} = -Da_C\tilde{Y}_F^p\tilde{Y}_{O_2}^q\exp\left(-\frac{\tilde{T}_a}{\tilde{T}}\right) \tag{1.93}$$

where Da_C is a Damköhler number

$$Da_C = \frac{2r_s^q B\hat{\rho}_{st}^{p+q-1}Y_{F,1}^{p+q-1}}{\chi_{st}M_F^p M_{O_2}^q} \tag{1.94}$$

For future reference, the diffusion transport operator on the left hand side of these equations is denoted by $\tilde{L}$

$$\tilde{L} \equiv \frac{\mathrm{d}^2}{\mathrm{d}Z^2} \tag{1.95}$$

1.6.1 Inner expansions

As is customary in Large Activation Energy Asymptotics (AEA) [13], [21], a small parameter for the reaction zone is defined as

$$\epsilon = \frac{\tilde{T}_{st}^2}{\tilde{T}_a} \tag{1.96}$$

A stretching transformation is introduced for the mixture fraction around $Z = Z_{st}$

$$Z = Z_{st} + \epsilon\tilde{Z} \tag{1.97}$$

and inner expansions are postulated for the flame temperature and mass concentrations

$$\begin{aligned}\tilde{Y}_F &= \epsilon \mathscr{Y}_F + O(\epsilon^2) \\ \tilde{Y}_{O_2} &= \epsilon \mathscr{Y}_{O_2} + O(\epsilon^2) \\ \tilde{T} &= \hat{T}_{st} - \epsilon \mathscr{T} + O(\epsilon^2)\end{aligned} \tag{1.98}$$

In the foregoing equations, fuel and oxidizer are assumed to vanish at the flame zone to leading order, and the leading order flame temperature is dictated by that given by the outer solutions, with which they are matched (containing radiation effects). However, the reaction rate varies rapidly in the inner region, its variations are governed by the first order term owing to the large Damköhler number. From a dominant balance of the terms involved, one may write the inner energy equation as

$$\frac{\mathrm{d}^2 \mathscr{T}}{\mathrm{d}\tilde{Z}^2} = Da_C \epsilon^{p+q+1} \mathscr{Y}_F^p \mathscr{Y}_{O_2}^q \exp\left(-\frac{\tilde{T}_a}{\tilde{T}}\right) \tag{1.99}$$

In the foregoing equation, radiation is neglected in comparison with the reaction term. Length scale arguments may be invoked to compare the two terms; the length scale over which radiation effects become important are much larger than that of the reaction zone.

After expanding the temperature in the exponential term using equation (1.98), and grouping constants together one gets

$$\frac{\mathrm{d}^2 \mathscr{T}}{\mathrm{d}\tilde{Z}^2} = \delta \mathscr{Y}_F^p \mathscr{Y}_{O_2}^q \exp(-\mathscr{T}) \tag{1.100}$$

where δ is a reduced Damköhler number defined as

$$\boxed{\delta = Da_C \epsilon^{p+q+1} \exp\left(-\frac{\tilde{T}_a}{\hat{T}_{st}}\right)} \tag{1.101}$$

which works out as

$$\boxed{\delta = \frac{2\hat{\rho}_{st}^{p+q-1} Y_{F,1}^{p+q-1} r_s^q A \exp(-T_a/\hat{T}_{st}) \epsilon^{p+q+1}}{(10^6)^{p+q-1} M_F^{p-1} M_{O_2}^q \chi_{st}}} \tag{1.102}$$

Extinction conditions are interpreted from the foregoing equation as occuring when the ODE for the flame temperature implied ceases to have a solution. This shall be elaborated upon later. One wishes (in equation (1.100)) to express the mass fraction terms $\mathscr{Y}_F$ and $\mathscr{Y}_{O_2}$ in terms of the inner temperature quantity $\mathscr{T}$. This is done by using Shvab-Zeldovich relationships and matching with the outer solutions. Consider the coupling relationship around $Z = Z_{st}$

$$\tilde{L}(\tilde{T} + \tilde{Y_F}) = \frac{2}{\rho Y_{F,1} \chi \Delta H_F} \nabla \cdot \vec{q}_R \tag{1.103}$$

Upon decomposing into inner scales one gets

$$\frac{\mathrm{d}^2(\mathscr{T} + \mathscr{Y}_F)}{\mathrm{d}\tilde{Z}^2} = \epsilon \frac{2}{\rho_{st} Y_{F,1} \chi_{st} \Delta H_F} \nabla \cdot \vec{q}_R \tag{1.104}$$

By dominant balance, the RHS may be neglected in comparison with LHS, so that one has to leading order

$$\frac{\mathrm{d}^2(\mathscr{Y}_F - \mathscr{T})}{\mathrm{d}\tilde{Z}^2} = 0 \tag{1.105}$$

which has the solution

$$\mathscr{Y}_{\mathscr{F}} - \mathscr{T} = C_1 \tilde{Z} + C_2 \tag{1.106}$$

Or in other words, around $Z = Z_{st}$ one has

$$\tilde{T} + \tilde{Y}_F = C_1 Z + C_3 \tag{1.107}$$

where

$$C_3 = \tilde{T}_{st} - C_1 Z_{st} + \epsilon C_2 \tag{1.108}$$

Differentiating on the air side, putting $Y_F(Z \to Z_{st,-}) = 0$, and matching with outer solutions

$$C_1 = \left(\frac{\mathrm{d}\tilde{T}}{\mathrm{d}Z}\right)_{Z=Z_{st,-}} = \left(\frac{\mathrm{d}\hat{T}}{\mathrm{d}Z}\right)_{Z=Z_{st,-}} \tag{1.109}$$

In order to obtain C_2 comparison is made with the Shvab-Zeldovich relationship that constitutes $\tilde{T} + \tilde{Y}_F$.

$$L'(T' + Y_F') = \frac{1}{\alpha\rho\Delta H_F}\nabla \cdot \vec{q}_R \tag{1.110}$$

The right hand side is a function of the temperature, and one would expect the solution at the flame to be embedded in an integral kernel with the corresponding Green's function. Note is made of the fact that the integral kernel will be a function (in order of magnitude terms) of an average absorption coefficient.

$$\frac{1}{\alpha\rho}\nabla \cdot \vec{q}_R \sim \frac{\sigma T_f^4}{\alpha\rho_f\Delta H_F}\bar{\kappa}[1 + O(\epsilon)] \tag{1.111}$$

where $\bar{\kappa}$ is some average absorption coefficient for the system. In the absence of radiation, this quantity is zero (putting $\bar{\kappa} = 0$), which gives $C_2 = 0$ when a term by term comparison in equation (1.108) is carried out, yielding the so-called Burke-Schuman solution. However, when κ is non-zero, the $O(1)$ term gives a measure of the temperature drop arising from radiation (which is what is computed in the outer solutions). In this case, one expects a contribution from the $O(\epsilon)$ term when there is radiation, which would increase in significance as $\bar{\kappa}\ell$ (in rough terms, ℓ contains the effect of strain) increases. In the current analysis, it is neglected for simplicity (as would indeed be the case, when $\bar{\kappa}\ell$ is small). Hence, the analysis is to some extent valid mostly for *small* $\bar{\kappa}\ell$. We carry out the analysis with this assumption,

and compare them with the DNS solutions obtained for validation. A successful validation would imply that it is reasonable to neglect the higher order terms.

This also brings to focus an interesting question regarding the formulation of the inner approximations in optically thicker media, where the laminar flamelet equations would have to be revisited in strongly radiating flames, since the inner equations will take a different form from what is usually presented [24, 25, 14] (note is made of the fact that these references consider only optically thin conditions, and that this issue has not hitherto been raised, to the best of the author's recollection, anywhere else). By logical extension of the above arguments, it becomes apparent that extinction conditions will hardly have the same morphological features as the 'classical' extinction conditions, because these arise from an entirely different type of inner equation, and therefore, one which will have a different solution for the Damköhler number. However, whether or not such conditions arise in practice is moot, aside from providing a rather interesting theoretical minutia to cogitate over.

To return to the main point of the discussion, putting $C_2 = 0$ one gets

$$\mathscr{Y}_F = \mathscr{T} - \left(\frac{\mathrm{d}\hat{T}}{\mathrm{d}Z}\right)_{Z=Z_{st,-}} \tilde{Z} \tag{1.112}$$

Similarly, for the oxygen mass fraction one obtains

$$\mathscr{Y}_{O_2} = \mathscr{T} - \left(\frac{\mathrm{d}\hat{T}}{\mathrm{d}Z}\right)_{Z=Z_{st,+}} \tilde{Z} \tag{1.113}$$

Thus, the inner energy equation may be written as

$$\frac{\mathrm{d}^2\mathscr{T}}{\mathrm{d}\tilde{Z}^2} = \delta \left[\mathscr{T} - \left(\frac{\mathrm{d}\mathscr{T}}{\mathrm{d}\tilde{Z}}\right)_{Z_{st,-}} \tilde{Z}\right]^p p \left[\mathscr{T} - \left(\frac{\mathrm{d}\mathscr{T}}{\mathrm{d}\tilde{Z}}\right)_{Z_{st,+}} \tilde{Z}\right]^q \exp(-\mathscr{T}) \tag{1.114}$$

1.6.1.1 Transformation into Liñan's form

It is convenient to transform the inner equations into the form given in Liñan [13], which may be achieved as follows.

Define

$$\begin{aligned} \theta &= \mathscr{T} - \left[\left(\frac{\mathrm{d}\hat{T}}{\mathrm{d}Z}\right)_{Z_{st,+}} + \left(\frac{\mathrm{d}\hat{T}}{\mathrm{d}Z}\right)_{Z_{st,-}}\right]\frac{\tilde{Z}}{2} \\ \eta &= \left[\left(\frac{\mathrm{d}\hat{T}}{\mathrm{d}Z}\right)_{Z_{st,+}} - \left(\frac{\mathrm{d}\hat{T}}{\mathrm{d}Z}\right)_{Z_{st,-}}\right]\frac{\tilde{Z}}{2} \end{aligned} \tag{1.115}$$

and

$$\gamma = \frac{\left(\frac{\mathrm{d}\hat{T}}{\mathrm{d}Z}\right)_{Z_{st,+}} + \left(\frac{\mathrm{d}\hat{T}}{\mathrm{d}Z}\right)_{Z_{st,-}}}{\left(\frac{\mathrm{d}\hat{T}}{\mathrm{d}Z}\right)_{Z_{st,+}} - \left(\frac{\mathrm{d}\hat{T}}{\mathrm{d}Z}\right)_{Z_{st,-}}} \tag{1.116}$$

to get

$$\boxed{\frac{\mathrm{d}^2\theta}{\mathrm{d}\eta^2} = \delta_*(\theta+\eta)^p(\theta-\eta)^q \exp[-(\theta+\gamma\eta)]} \tag{1.117}$$

where δ_* is a reduced Damköhler number defined as

$$\delta_* = \frac{4\delta}{\left[\left(\frac{\mathrm{d}\hat{T}}{\mathrm{d}Z}\right)_{Z_{st,+}} - \left(\frac{\mathrm{d}\hat{T}}{\mathrm{d}Z}\right)_{Z_{st,-}}\right]^2} \tag{1.118}$$

The boundary conditions for this problem are

$$\boxed{\left(\frac{\mathrm{d}\theta}{\mathrm{d}\eta}\right)_{\eta\to-\infty} = -1; \qquad \left(\frac{\mathrm{d}\theta}{\mathrm{d}\eta}\right)_{\eta\to\infty} = 1} \tag{1.119}$$

1.6.2 Extinction conditions

Extinction is interpreted as occurring when equation (1.117) ceases to have a solution for a given value of δ_*. This happens when δ_* becomes small. From the test cases carried out here, it is seen that this happens when $\delta_* \approx 1$. To understand

this better, inspection is made of the reduced Damköhler number δ_*

$$\delta_* = \frac{4\delta}{\left[\left(\frac{\mathrm{d}\mathscr{T}}{\mathrm{d}\tilde{Z}}\right)_{Z_{st,+}} - \left(\frac{\mathrm{d}\mathscr{T}}{\mathrm{d}\tilde{Z}}\right)_{Z_{st,-}}\right]^2}$$

In the foregoing, the denominator is the jump condition in the outer temperature gradient, which is a constant. This is because the temperature drop from radiation is assumed to be a smooth function in temperature, and gets canceled out, yielding the same jump condition as in the adiabatic case. It is esentially a measure of the strength of the chemical reaction, as shall be shown subsequently. One can therefore say that $\delta_* \sim \delta$. Investigation of the functional form of δ provides some insight into the phenomenology of extinction.

$$\delta \sim Da_C \epsilon^{p+q+1} \exp\left(-\frac{\tilde{T}_a}{\hat{T}_{st}}\right) \sim \frac{1}{\chi_{st}} \epsilon^{p+q+1} \exp\left(-\frac{\tilde{T}_a}{\hat{T}_{st}}\right) \tag{1.120}$$

Extinction conditions occur when $\delta_* < \delta_{*,C}$ where $\delta_{*,C} \approx 1$. This would happen when

- the scalar dissipation rate (appears in the denominator in the expression for Da_C) becomes large-as would be expected when the flame is strongly stretched.
- the flame temperature (appears in the exponential term) becomes small-as would happen in strongly radiating flames.

It is noted that radiating conditions only affect the value of γ, which depends on the temperature jump conditions at the flame. That $\delta_* \approx 1$ for extinction supports the idea that one could write an extinction model back-calculate the extinction flame temperature for a given stretch rate.

1.6.3 The strength of the reaction source term

The reaction source term at the flame may be obtained from the outer solutions, which are sufficient to determine the burning rate as follows. Consider the inner equation in mixture fraction coordinates.

$$\frac{\mathrm{d}^2 Y_F}{\mathrm{d}Z^2} = \frac{2}{\rho_{st}\chi_{st}}\dot{\omega}_F \tag{1.121}$$

This equation may be integrated to give the burning rate.

$$\left[\left(\frac{\mathrm{d}Y_F}{\mathrm{d}Z}\right)_{Z_{st,+}} - \left(\frac{\mathrm{d}Y_F}{\mathrm{d}Z}\right)_{Z_{st,-}}\right] = \frac{2}{\rho_{st}\chi_{st}}\int_{Z_{st,-}}^{Z_{st,+}} \dot{\omega}_F \mathrm{d}Z \tag{1.122}$$

which yields

$$\left[\left(\frac{\mathrm{d}Y_F}{\mathrm{d}Z}\right)_{Z_{st,+}} - \left(\frac{\mathrm{d}Y_F}{\mathrm{d}Z}\right)_{Z_{st,-}}\right] = \frac{2}{\rho_{st}\chi_{st}}\left(\frac{\mathrm{d}Z}{\mathrm{d}x}\right)_{st}\int_{x_{st,-}}^{x_{st,+}} \dot{\omega}_F \mathrm{d}x \tag{1.123}$$

Rewriting, and recognizing that

$$\chi_{st} = 2D_{st}\left(\frac{\mathrm{d}Z}{\mathrm{d}x}\right)_{st}^2 \tag{1.124}$$

together with $\rho_{st}^2 D_{st} = \rho_2^2 D_2$ one gets

$$\int_{x_{st,-}}^{x_{st,+}} \dot{\omega}_F \mathrm{d}x = \left[\frac{\mathrm{d}Y_F}{\mathrm{d}Z}\right]_{st}\sqrt{\frac{D_2}{2}}\sqrt{\chi_{st}} \tag{1.125}$$

where

$$\left[\frac{\mathrm{d}Y_F}{\mathrm{d}Z}\right]_{Z_{st,-}}^{Z_{st,+}} = \left[\left(\frac{\mathrm{d}Y_F}{\mathrm{d}Z}\right)_{Z_{st,+}} - \left(\frac{\mathrm{d}Y_F}{\mathrm{d}Z}\right)_{Z_{st,-}}\right] \tag{1.126}$$

is the fuel mass jump condition. This may be used to shed insight into fuel and oxidizer vitiation by noting its on the boundary conditions $Y_{F,1}$ and $Y_{O_2,2}$).

Invoking the solution for the Burke-Schuman flame, we get

$$\begin{aligned} Y_F &= 0; && Z < Z_{st} \\ &= Y_{F,1}\frac{Z - Z_{st}}{1 - Z_{st}}; && Z \geq Z_{st} \end{aligned} \tag{1.127}$$

or

$$\left[\frac{\mathrm{d}Y_F}{\mathrm{d}Z}\right]_{st} = \frac{Y_{F,1}}{1-Z_{st}} = Y_{F,1} + Y_{O_2,2}/r_s \tag{1.128}$$

which gives

$$\boxed{\int_{x_{st,-}}^{x_{st,+}} \dot{\omega}_F \mathrm{d}x = \sqrt{\frac{D_2}{2}}\left(Y_{F,1} + Y_{O_2,2}/r_s\right)\sqrt{\chi_{st}}} \tag{1.129}$$

The above expression should hold (in the fast chemistry regime) for a general turbulent flame, requiring information on the local flow conditions, embedded in the scalar dissipation rate χ_{st}; and the ambient mixing conditions, which we would expect to be affected by vitiation of fuel and oxidizer, and which are embodied in the quantity containing the fuel and oxidizer ambient mass fractions. This expression is subjected to a verification test using data obtained from DNS.

1.7 Flame structure using soot

Soot formation is described using a phenomenological modeling strategy previously developed by Moss *et al.* [18, 5] and Lindstedt *et al.* [12, 10]. The strategy consists in solving two transport equations for soot mass fraction Y_{soot} and soot number density N_{soot}:

$$(\bar{u} + \bar{V}_t)\frac{\mathrm{d}Q}{\mathrm{d}\xi} + \frac{\mathrm{d}\bar{V}_t}{\mathrm{d}\xi} = \frac{\dot{\omega}_Q}{\rho} \tag{1.130}$$

where Q is Y_{soot} or $n_{soot}/(\rho/N_A)$ with N_A the Avogadro number, $N_A = 6.022 \times 10^{26}$particles/mol, and where $\bar{V}_t$ is the density weighted thermophoretic velocity in the flame normal direction

$$V_t = -0.54\nu_2\frac{\partial}{\partial\xi}(\ln T) \tag{1.131}$$

with ν_2 the kinematic viscosity in the oxidizer stream. The source term on the RHS of equation (1.130) incorporates semi-empirical descriptions of important physical and chemical soot processes, e.g. particle inception, surface growth, oxidation, and coagulation [5, 12, 10]. These expressions are also based on a number of simplifying assumptions, for instance the model ignores the role of soot precursors and assumes a mono-dispersed soot particle size distribution. In addition, because it is combined with single-step combustion chemistry, the model adopts ethylene as the controlling species for soot inception and O_2 as that for soot oxidation. Model coefficients are taken from [5]. The values of the fuel and oxygen mole fractions and of temperature required in equation (1.130) are obtained from a reconstructed flame solution that combines the inner and outer solutions discussed in 1.6: the inner solution is used for $Z_{st} - 0.01 \leq Z \leq Z_{st} + 0.02$; the outer solution is used outside that range. Equation (1.130) is solved using a second order finite difference method and is coupled to the outer and inner equations via an interative algorithm.

Soot mass is added to the flow on the air side of the flame. While adding soot on the fuel side may appear as a better representation of the multi-dimensional sooting flame configurations that motivate the present study, it is important to realize that since the counterflow flame is located on the air side of the stagnation plane,soot particles added to the fuel will essentially follow flow streamlines and will never reach the flame because of the adverse effects of convection and thermophoresis; thus, to evaluate their impact on flame structure, soot particles must be added at locations where they can be convected into the reaction zone. This observation illustrates some of the challenges found in using counterflow flame configurations as

a representative model for sooting flames.

1.8 Results

The flame structure was calculated using the AEA formulation presented in 1.4 and for different strain rate conditions while systematically changing these conditions until the extinction limits were reached (the limits are simply identified by the absence of numerical convergence). The calculations were also performed for different soot mass loading levels; the soot loading level is characterized by the value of the soot mass fraction upstream of the flame, noted $Y_{soot,R}$; the corresponding soot number density is not important and is arbitrarily chosen as a very small number. The selected values for $Y_{soot,R}$ are up to 5%, ; these values are believed to be representative of non-local soot loading effects in multi-dimensional flames: for instance, the case leads to values of the soot mass fraction in the flame region that are comparable to values previously observed in direct numerical simulations of turbulent flames [19].

Figure (1.3) presents the variations of peak flame temperature with strain rate α for three different soot loading levels. Similar variations for the corresponding adiabatic flame case are also included for comparison. The figure shows that the flammable domain of laminar counterflow diffusion flames is limited by upper and lower limits at large and low values of α. As discussed in 1.1, the upper limit corresponds to the classical flame response to increasing mixing rates, i.e. to an intensification of combustion at moderate-to-high values of α (or equivalently χ_{st}),

followed by aerodynamic quenching once $\alpha \geq \alpha^{UL}$ (or $\chi_{st} \geq \chi_{st}^{UL}$). This upper limit is the only extinction limit observed under adiabatic combustion conditions. The lower limit corresponds to the flame response to decreasing mixing rates, i.e. to a progressive weakening of combustion at moderate-to-low values of α, followed by radiative extinction once $\alpha \leq \alpha^{LL}$ ($\chi_{st} \leq \chi_{st}^{LL}$). In the absence of soot loading ($Y_{soot,R} = 0$), we find: $\alpha^{LL} \approx 0.8$ s^{-1} ($\chi_{st}^{UL} \approx 0.25$ s^{-1}) and $\alpha^{UL} \approx 1955$ s^{-1} ($\chi_{st}^{UL} \approx 61$ s^{-1}). In the case with $Y_{soot,R} = 0.05$, we find: $\alpha^{LL} \approx 13$ s^{-1} ($\chi_{st}^{LL} \approx 0.4$ s^{-1}) and $\alpha^{UL} \approx 1360$ s^{-1} ($\chi_{st}^{UL} \approx 42$ s^{-1}). Thus, we find that soot mass loading results in a significant decrease of the size of the flammable domain, and that for the range of conditions considered in the present study, the maximum value of flame stretch at the upper extinction limit may be decreased by as much as 30% while the minimum value of flame stretch at the lower limit may be increased by more than an order of magnitude.

These modifications of the flammable domain in the presence of soot loading are further illustrated in Figure 1.4. Figure 1.4 presents the variations of the Damköhler number with δ_* and α shows that consistent with classical laminar flame theory, flame extinction occurs when δ_* takes critically low values. An important result in Figure 1.4 is that the critical values of δ_* at the lower limit are approximately equal to those at the upper limit: in the case with $Y_{soot,R} = 0$, $\delta_*^{LL} \approx 1.1$ and $\delta_*^{UL} \approx 1.2$, whereas in the case with $Y_{soot,R} = 0.05$, $\delta_*^{LL} \approx 0.9$ and $\delta_*^{UL} \approx 1.2$, with δ_*^{LL} (δ_*^{UL}) the value of δ_* at the lower (upper) extinction limit. This result lends support to the unifying concept of a flame Damköhler number as the basis to predict all flame extinction limits: an approximate but reasonably accurate expression of

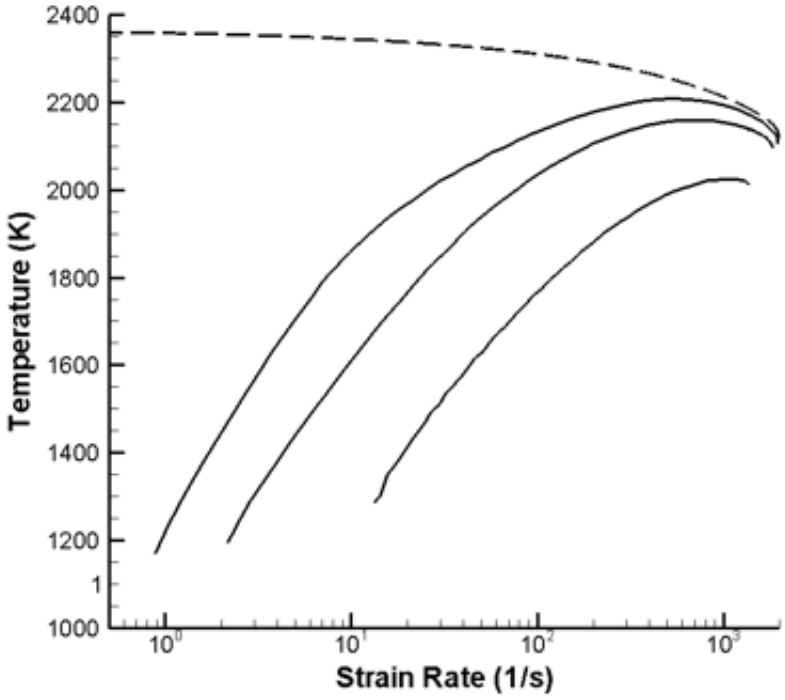

Figure 1.3: Peak flame temperature versus strain rate α (log-linear plot). Top dashed line: adiabatic flame. Three lower solid lines: sooting and radiating flames with $Y_{soot,R} = 0$ (top), 1% (middle), 5% (bottom). The end points of each solid line mark the lower and upper limits of the flammable domain.

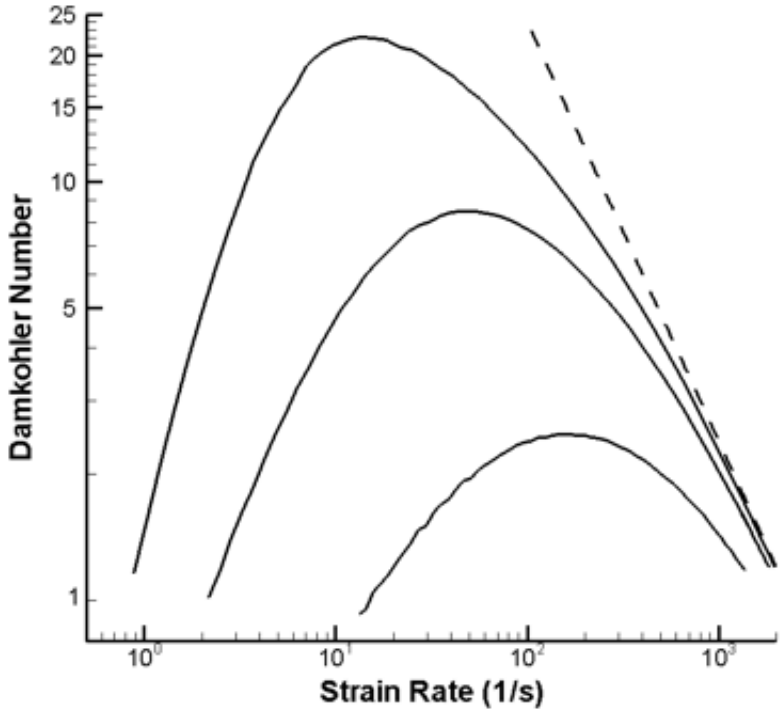

Figure 1.4: Damköhler number versus strain rate α (log-log plot). Top dashed line: adiabatic flame. Three lower solid lines: sooting and radiating flames with $Y_{soot,R} = 0$ (top), 1% (middle), 5% (bottom). The critical values of at the extinction limits are close to 1.

the extinction criterion is $\delta_* \leq 1$.

Figure 1.5 presents the variations of soot volume fraction $f_{v,st}$ with strain rate α; $f_{v,st}$ is the soot volume fraction measured at the stoichiometric location where $Z = Z_{st}$. In the absence of soot loading, significant amounts of soot may be produced on the fuel side of the flame but this soot mass does not accumulate in the high temperature region of the flame because of adverse effects of both oxidation chemistry and convective and thermophoretic transport: $f_{v,st}$ remains below 0.01 ppm.

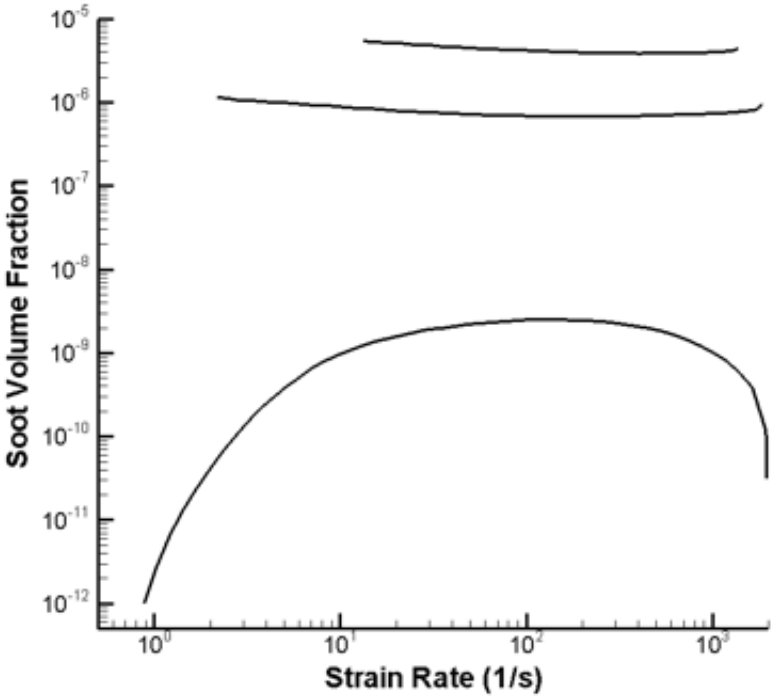

Figure 1.5: Stoichiometric value of the soot volume fraction $f_{v,st}$ versus strain rate α (log-log plot). Three solid lines: sooting and radiating flames with $Y_{soot,R} = 0$ (bottom), 1% (middle), 5% (top).

In contrast, in the presence of soot loading, there are significant amounts of soot mass present in the high temperature region of the flame: $f_{v,st}$ is on the order of 1 ppm in the case with $Y_{soot,R} = 0.01$, and on the order of 5 ppm in the case with $Y_{soot,R} = 0.05$. This high-temperature soot is responsible for the increase in the flame luminosity and for the associated changes in the flame dynamics described in Figures 1.3, 1.4.

Figures 1.6, 1.7, 1.8 present two representative flame structures, as obtained for $\alpha = 20$ s^{-1}, with and without external soot loading. Under these low strain rate

conditions, the effects of radiation cooling are pronounced and are responsible for a dramatic decrease in peak flame temperature equal to approximately 330 K when and 500 K when $Y_{soot,R} = 0.02$ (Figure 1.6).

Figure 1.7 presents the corresponding spatial variations of soot volume fraction across the flame. In the case with $Y_{soot,R} = 0.02$, the soot mass is released upstream of the flame at $x \approx 17$ mm. As they approach the flame zone (i.e., moving from right to left in 1.7), a significant fraction of the soot particles is first consumed by oxidation (a consequence of adding soot on the air side of the flame); the rest is transported across the reaction zone where as mentioned above, the particles contribute to increasing the flame luminosity and to weakening the flame.

Figure 1.8 presents the corresponding spatial variations of the mean absorption coefficient κ. In the absence of soot loading, the flame optical depth τ_R takes low values $\tau_R \approx 0.035$, and the flame remains in the optically-thin regime, i.e., a radiation regime dominated by emission; in contrast, in the case $Y_{soot,R} = 0.02$, $\tau_R \approx 0.12$, and the flame belongs to a mixed radiation regime in which absorption becomes important. Also, while in the case with $Y_{soot,R} = 0$, the contributions of soot and gas radiation to the mean absorption coefficient κ have comparable weights, in the case with $Y_{soot,R} = 0.02$, the soot contribution is clearly dominant.

In figure 1.9 comparison is made between the AEA results for the case with $Y_{soot,R} = 0$ and the correspondingly setup DNS case (with the notable difference that the DNS uses $\rho^{1.7} D = constant$). Also, for this comparison $C_{soot} = 700$ m^{-1}K^{-1} is used. It is analogous to Figure 1.3, but uses the stoichiometric values. The DNS simulations are carried out so that a *library* of 'flamelets' at various straining rates

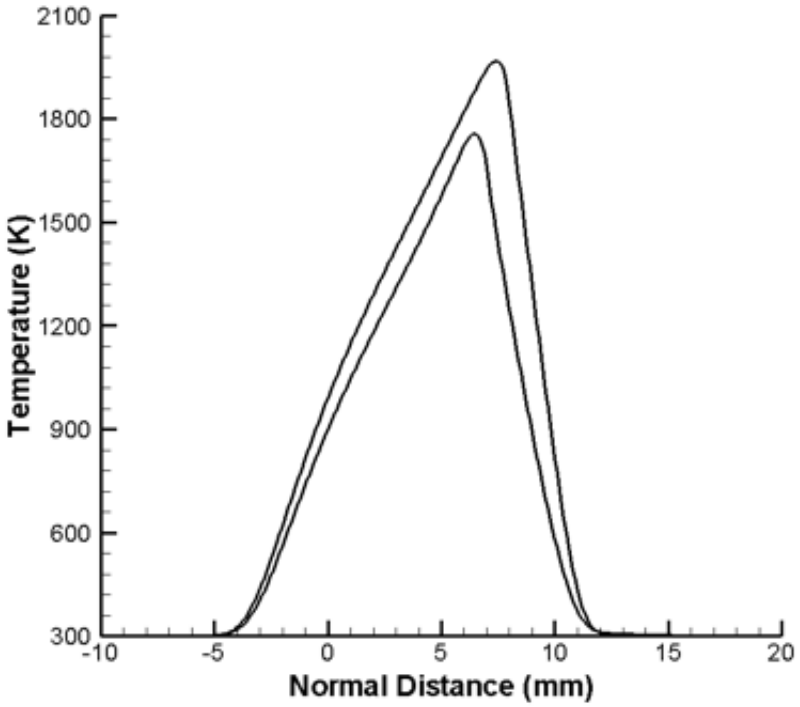

Figure 1.6: Temperature versus normal distance to the flame, $\alpha = 20s^{-1}$. Top line: flame with $Y_{soot,R} = 0$; bottom line: soot-loaded flame with $Y_{soot,R} = 2\%$. $x \leq 5$ mm corresponds to the fuel (air) side of the flame.

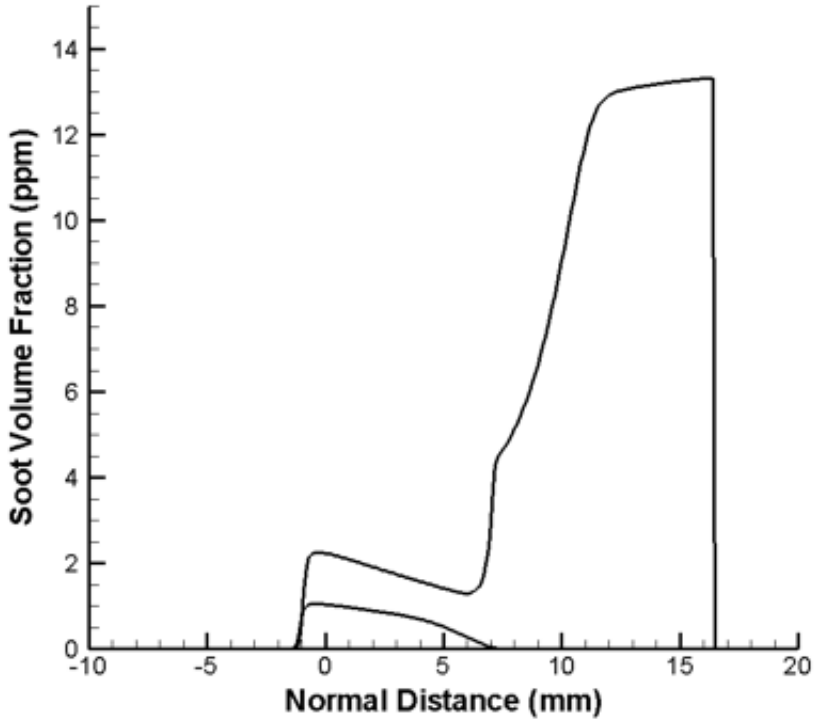

Figure 1.7: Soot volume fraction versus normal distance to the flame, $\alpha = 20s^{-1}$. Bottom line: flame with $Y_{soot,R} = 0$; top line: soot-loaded flame with $Y_{soot,R} = 2\%$. Soot addition occurs at $x \approx 17$ mm .

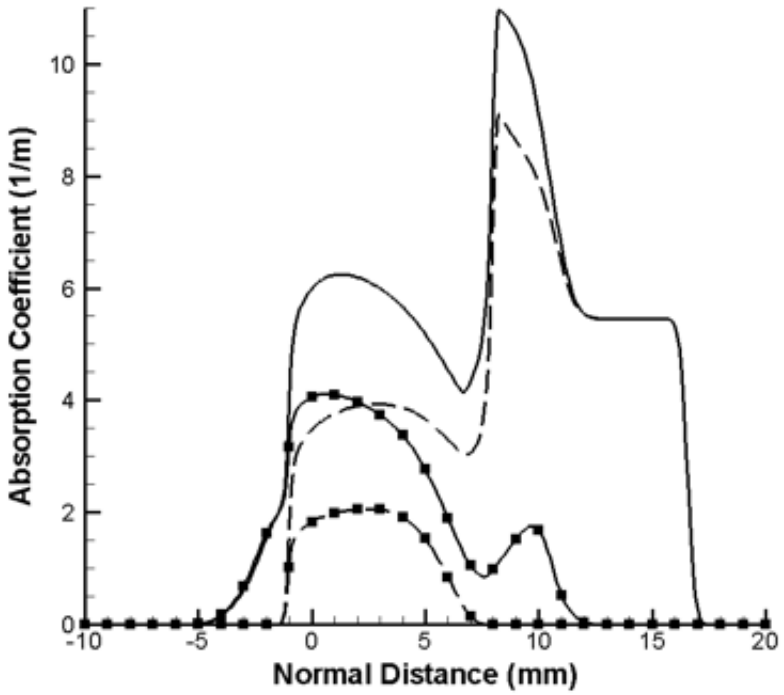

Figure 1.8: Mean radiation absorption coefficient versus normal distance to the flame, $\alpha = 20$ s^{-1}. Bottom lines with square symbols: flame with $Y_{soot,R} = 0$; top lines without symbol: soot-loaded flame with $Y_{soot,R} = 2\%$. For each flame case, the plot shows the total absorption coefficient κ (upper solid curve) and its soot contribution, (lower dashed curve); the difference between the two curves is the contribution of CO_2 and H_2O. (see Eq. (12)).

is generated-from the high stretch limit to the low stretch limit. The comparison between the two cases appears to be highly favorable over the whole range of straining conditions, thereby lending credence to the modeling assumptions made in the asymptotic formulation. Allusion is made to the point made regarding the correctness of the approximations made to the inner equation, which seems to be borne out from the numerical experiments. This aspect is not too surprising because the conditions simulated are for small optical thickness, where the approximations were deemed to be good. Also, the usage of $\rho^2 D = constant$, does not seem to lead to any degradation in solution quality, while simplifying the analytical treatment considerably.

1.9 Conclusions

The effect of external soot loading on the extinction limits of laminar counterflow ethylene-air diffusion flames is studied using large activation energy asymptotic theory. The AEA analysis is extended to include a phenomenological soot model that accounts for particles inception, growth and oxidation, and a generalized treatment of thermal radiation that accounts for both emission and absorption phenomena and applies to participating media ranging from optically-thin to optically-thick. Soot loading is simulated by adding a controlled amount of soot mass to the flow upstream of the flame.

The AEA analysis shows that soot loading results in a significant decrease of the size of the flammable domain: the minimum value of flame stretch at the radia-

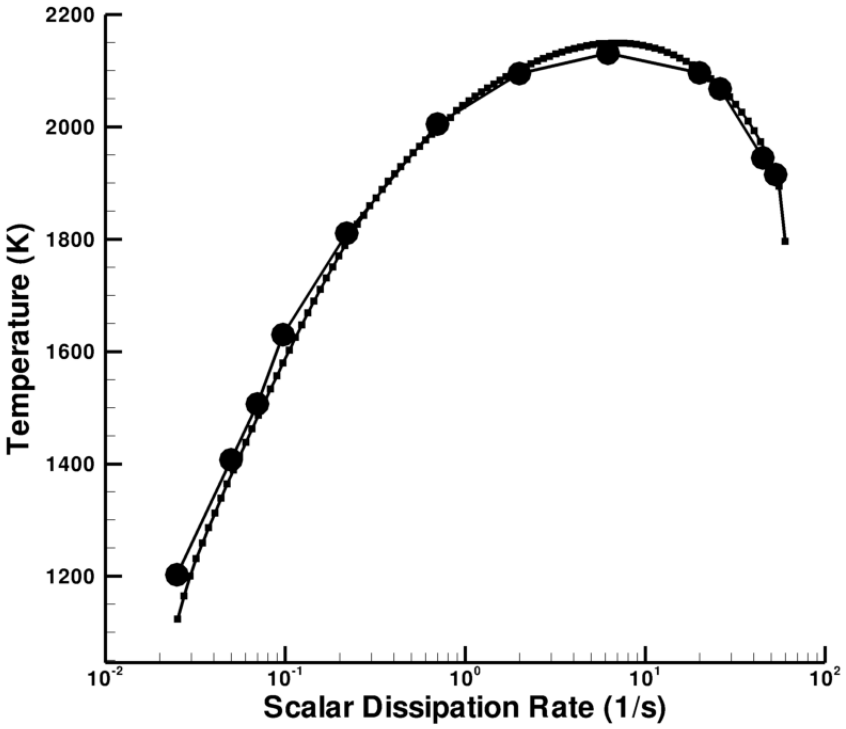

Figure 1.9: Flame temperature versus T_{st} versus scalar dissipation rate χ_{st} at stoichiometric location, with $Y_{soot,R} = 0$, compared between DNS (large circular symbols) and AEA (small square symbols). The end points of each line mark the lower and upper limits of the flammable domain.

tive extinction limit is increased by more than an order of magnitude. These results support the idea that in multi-dimensional sooting flames, soot first produced at locations characterized by fast fuel-air mixing and vigorous combustion conditions and then transported into locations characterized by slow mixing and sluggish combustion conditions will play a dominant role by increasing the local flame luminosity and driving the flame towards radiative extinction. This non-local multi-dimensional effect is believed to be a dominant mechanism to explain flame extinction in fires; this effect is not present in classical (i.e., non-soot-loaded) one-dimensional flame configurations, which suggests that these configurations are not representative of multi-dimensional sooting flame conditions.The present AEA results indicate that in multi-dimensional laminar or turbulent sooting flames, stretched flame elements with values of the strain rate above approximately 13 s^{-1} (or stoichiometric values of the scalar dissipation rate above 0.4 s^{-1}) will be susceptible to radiative extinction. The AEA results also support the concept of a single critical value of the Damköhler number to predict all flame extinction limits. Future work will consider an application of the present AEA analysis to the construction of flammability maps relevant to fire problems.

Bibliography

[1] *International Workshop on Measurement and Computation of Turbulent Non-premixed Flames* (Sandia National Laboratories). `http://public.ca.sandia.gov/TNF/radiation.html`.

[2] Bai, X, S., Fuchs, L., and Mauss, F. Laminar flamelet structure at low and vanishing scalar dissipation rate. *Combustion and Flame* (2000), 285–300.

[3] Baum, H, R. Notes on Howarth transformation. Private communication, 2009.

[4] Bender, C, M., and Orszag, S, A. *Advanced Mathematical Methods for scientists and engineers*. McGraw-Hill Book Company, 1978.

[5] Brookes, S, J., and Moss, J, B. Predictions of soot and thermal radiation properties in confined turbulent jet diffusion flames. *Combustion and Flame 116* (1999).

[6] Carrier, G, F., and Pearson, C, E. *Ordinary Differential Equations, Theory and Practice*. Classics in Applied Mathematics. SIAM, 1992.

[7] Carrier, G, K., Fendell, F, E., and Marble, F, E. The effect of strain rate on diffusion flames. *SIAM Journal of Applied Mathematics 28*, 2 (March 1975).

[8] Chan, S, H., Yin, J, Q., and Shi, B, J. Structure and extinction of methane-air flamelet with radiation and detailed chemical kinetic mechanism. *Combustion and Flame 112* (1998), 445–456.

[9] Daguse, T., Croenenbek, T., Rolon, J, C., Darabiha, N., and Soufiani, A. Study of radiative effects on laminar counterflow $H_2/O_2/N_2$ diffusion flames. *Combustion and Flame 106* (1996), 271–287.

[10] Fairweather, M., Jones, W, P., Ledin, H, S., and Lindstedt, R, P. Predictions of soot formation in turbulent, non-premixed propane flames. In *Proceedings of the Combustion Institute* (1992), vol. 24, pp. 1067–1074.

[11] Joulain, P. The behavior of pool fires: State of the art and new insights. In *Proceedings of the Combustion Institute* (1998), vol. 27, pp. 2691–2706.

[12] Leung, K, M., Lindstedt, R, P., and Jones, W, P. A simplified reaction mechanism for soot formation in nonpremixed flames. *Combustion and Flame 87* (1991), 289–305.

[13] Liñan, A. The asymptotic structure of counterflow diffusion flames for large activation energies. *Acta Astronautica 1007*, 1 (1974), 1–29.

[14] Liu, F., Smallwood, G, J., G'ulder, 'O, L., and Ju, Y. Asymptotic analysis of radiative extinction in counterflow diffusion flames of nonunity lewis numbers. *Combustion and Flame 121* (2000), 275–287.

[15] Markstein, G, H. Relationship between smoke point and radiant emission from buoyant turbulent and laminar diffusion flames. In *Proceedings of the Combustion Institute* (1985), vol. 20, pp. 1055–1061.

[16] Markstein, G, H., and de Ris, J. Radiant emission and absorption by laminar ethylene and propylene diffusion flames. In *Proceedings of the Combustion Institute* (1985), vol. 20, pp. 1637–1646.

[17] Maruta, K., Yoshida, M., Guo, H., Ju, Y., and Niioka, T. Extinction of low-stretched diffusion flame in microgravity. *Combustion and Flame 112* (1998), 181–187.

[18] Moss, J, B., Stewart, C, D., and Young, K, J. Modeling soot formation and burnout in a high temperature laminar diffusion flame burning under oxygen-enriched conditions. *Combustion and Flame 101* (1995), 491–500.

[19] Narayanan, P., and Trouvé, A. Radiation-driven flame weakening effects in turbulent diffusion flames. In *Proceedings of the Combustion Institute* (2009), vol. 32, pp. 1481–1489.

[20] Orloff, L., de Ris, J., and Delechatsios, J. Radiation from buoyant diffusion flames. *Combustion Science and Technology 84* (July 1992), 177–186.

[21] Peters, N. Local quenching due to flame stretch and non-premixed turbulent combustion. *Combustion Science and Technology 30* (1983), 1–17.

[22] Peters, N. *Turbulent combustion*. Cambridge university press, 2000.

[23] Rhatigan, J, H., Bedir, H., and T'ien, J, S. Gas-phase radiative effects on the burning and extinction of a solid fuel. *Combustion and Flame 112* (1998), 231–241.

[24] Sohrab, S, H., Liñan, A., and Williams, F, A. Asymptotic theory of diffusion-flame extinction with radiant loss from the flame zone. *Combustion Science and Technology 27* (1982), 143–154.

[25] Wang, H, Y., Chen, W, H., and Law, C, K. Extinction of counterflow diffusion flames with radiative heat loss and nonunity lewis numbers. *Combustion and Flame 148* (2007), 100–116.

[26] Westbrook, C, K., and Dryer, F, L. Simplified reaction mechanism for the oxidation of hydrocarbon fuels in flames. *Combustion Science and Technology 27* (1981), 31–43.

[27] Williams, F, A. *Combustion Theory*. Benjamin Cummings, Menlo Park, CA, 1985.